Coupling of Wave Data and Underwater Acoustic Measurements in a Maritime High-Traffic Coastal Area: A Case Study in the Strait of Sicily

FRANCESCO RAFFA,[a] GIOVANNI LUDENO,[b] GIUSEPPA BUSCAINO,[c] GIANMARIA SANNINO,[d] ADRIANA CARILLO,[d] ROSARIO GRAMMAUTA,[c] DOMENICO SPOTO,[c] FRANCESCO SOLDOVIERI,[b] SALVATORE MAZZOLA,[c] AND FRANCESCO SERAFINO[e]

[a] *Institute for Coastal Marine Environment, National Research Council, Messina, Italy*
[b] *Institute for Electromagnetic Sensing of the Environment (IREA), National Research Council, Napoli, Italy*
[c] *Institute for Coastal Marine Environment, National Research Council, Campobello di Mazara, Italy*
[d] *Climate Modeling and Impacts Laboratory, Italian National Agency for New Technologies, Energy and Sustainable Economic Development, Rome, Italy*
[e] *Institute of Biometeorology (IBMET), National Research Council, Florence, Italy*

(Manuscript received 16 March 2017, in final form 8 August 2017)

ABSTRACT

Underwater acoustic monitoring combined with real-time sea surface observations and numerical model forecasts could improve the efficiency of natural and anthropogenic sound source discrimination. In this work, acoustic sound pressure levels at different frequencies were compared with significant wave heights, measured using an X-band radar system, and then matched against independent data derived from a Simulating Waves Nearshore (SWAN) model in order to confirm their reliability. The acoustic data were recorded from a fixed buoy located in the Sicilian Channel at 4.9 km from the coast and 33 km from the X-band radar system installed at Cape San Marco (in the southwest region of Sicily). All data were acquired during two different periods: 28 February–16 March 2015 and 23 April–27 May 2015. The level of noise at the 16-Hz octave band showed the best linear correlation ($R = 0.78$), with in situ radar observations of significant wave height. Radar measurements of wave height coupled with in situ acoustic measurements give a characterization of the level of noise as result of sea state in a specific area. These measurements could be used to discriminate natural sources of noise (waves) from other sound sources, such as biological and anthropogenic sources. This discrimination contributes to understanding the impact of acoustic pollution on marine environments and provides a monitoring plan protocol for safeguarding biodiversity in the Mediterranean coastal areas.

1. Introduction

The monitoring of sea sounds and sea wave heights in coastal areas is more challenging than in the open sea, because of correlations occurring between these factors on a smaller spatial scale. Indeed, in coastal environments it is extremely difficult to measure sea sound levels and sea waves with the accuracy and spatial resolution required by numerical models for weather forecasting, which are useful also for safety at sea and coastal defense. Natural abiotic underwater sounds in coastal areas are determined mainly by waves, including breaking surface waves (Haxel et al. 2013), rainfall (Prosperetti and Oguz 1993) and waves beating against cliffs. Surface waves cause mostly infrasonic noise at frequencies from 10 to 100 Hz (Haxel et al. 2013). Their sources are interrelated although surf noise, which is defined as wave noise localized near the land–sea surface, is prominent. Rainfall produces energy peaks from 15 to 20 kHz (Nystuen 1986), while thunder and lightning can produce sounds at lower frequencies that contribute to background noise even when the locality of the storm is at considerable distances (Cotter 2009).

Anthropogenic noise in coastal areas could represent an important component of underwater sound level (Buscaino et al. 2016) and could negatively impact many marine organisms (Filiciotto et al. 2014; Celi et al. 2016; Buscaino et al. 2010; Sarà et al. 2007). Anthropogenic noise is mainly due to vessel traffic, particularly at low frequencies (<1 kHz) (Hildebrand 2009). Despite its high level of biodiversity (Myers et al. 2000), the Mediterranean Sea is affected by heavy traffic, and especially at lower frequencies, the Strait of Sicily, the principal corridor between the eastern and western basins, is characterized by heavy acoustic pollution (Buscaino et al. 2016).

Corresponding author: Francesco Raffa, francesco.raffa@cnr.it

DOI: 10.1175/JTECH-D-17-0046.1

Characterizing and evaluating the contributions of natural and anthropogenic sources is crucial for assessing the impact of human-made disturbances on marine habitats (Haxel et al. 2013; Hildebrand 2009). The European Union Marine Strategy Framework Directive (European Parliament, Council of the European Union 2008) promotes the achievement of good environmental status of European waters by 2020. In particular, Descriptor 11.2 regarding ''continuous low frequency sound'' aims to monitor trends in the ambient noise level within one-third octave bands (Maccarrone et al. 2015). In the assessment of good-quality environmental status, it has become fundamental to distinguish the contribution to ambient noise level of abiotic natural sound from that of anthropogenic sound. In fact, the simple monitoring of acoustic trends within one-third octave bands does not distinguish noise from vessel traffic (anthropogenic acoustic pollution) from noise caused by waves (natural noise); that is, an area could be very ''naturally'' noisy because of the effect of exposition to high waves although it is very far from vessel traffic and vice versa. Therefore, in the development of a noise-monitoring plan in marine shallow waters, a comparative study coupling wave data and underwater acoustic measurements contributes to distinguishing the main natural abiotic underwater noise from anthropogenic noise (Buscaino et al. 2016).

X-band marine radars are useful active microwave remote sensing systems for sea-state monitoring either offshore or close to the coastline. Sea surface analyses by marine radar are based on the acquisition of consecutive radar images. The sea surface in radar images is affected by a number of distortions, known as modulation effects (i.e., shadowing, tilt modulation, hydrodynamic modulation), that depend on both sea state (wavelength, wave height, and wave direction) and radar parameters (e.g., the space–time resolution of radar data), as well as on acquisition geometry (e.g., the radar height) (Plant and Keller 1990; Lee et al. 1995; Wenzel 1990; Carratelli et al. 2007; Pugliese Carratelli et al. 2006). To retrieve hydrodynamic parameters such as period, wavelength, direction of the dominant waves, and significant wave height, as well as surface current and bathymetry from a sequence of radar images, an inversion procedure is necessary (Nieto Borge et al. 2004; Serafino et al. 2010). A key element of the inversion procedure is the estimation of the surface current and bathymetry from the radar data, since the knowledge of these quantities makes it possible to build a bandpass (BP) filter to separate out background noise with respect to the spectral energy associated with wave motion.

Over the last two decades, several approaches for current and bathymetry estimation have been developed, such as the least squares (LS) (Young et al. 1985), the iterative least squares (ILS) (Senet et al. 2001), the normalized scalar product (NSP) (Serafino et al. 2010), and polar current shell (PCS) (Shen et al. 2015). In particular, in Huang and Gill (2012) the performances of the LS, ILS, and NSP approaches were compared with an ADCP under low state; the comparison pointed out that the NSP method provided the best results in terms of agreement with the buoy.

In the inversion procedure, after building the BP filter, the following step consists of applying a modulation transfer function (MTF) to convert the filtered radar spectrum into the desired sea wave spectrum; finally, it is possible to derive the abovementioned hydrodynamic parameters (Nieto Borge et al. 2004; Ludeno et al. 2014a; Lund et al. 2014; Fucile et al. 2016). Therefore, some estimated hydrodynamic parameters—for example, significant wave height—need a calibration using an external reference, such as the wave buoy. The most commonly used methods to derive significant wave height from radar images are based on the analysis of the zero-order moment of the wave spectrum and on that of the signal-to-noise ratio (SNR) between the spectral wave energy and the background noise component (Nieto Borge 1997; Nieto Borge et al. 2004; Nieto Borge and Guedes Soares 2000). Another possible strategy that also makes use of the peak wavelength and the mean wave period is based on multilayer perceptions (Vicen-Bueno et al. 2012). However, the problem of estimating the significant wave height from radar data has still not been completely solved, since most of the methods require some data provided by external references to be used for calibration purposes. A way to overcome this issue is shown in Gangeskar (2014), Salcedo-Sanz et al. (2015), and Liu et al. (2016), where a method to get the significant wave height from the analysis of shadowing occurring in radar images without any reference measurement was proposed.

A number of wave models are actually used for forecasting systems at global and local scales. Most of these models are spectral models based on the representation of the sea state through the energy spectrum, discretized in terms of frequencies and propagation directions. The evolution of the spectrum in space and time is computed by means of the energy balance equation, where the forcing is represented by sources and sinks of the wave energy, which are wind input, dissipation, and nonlinear interactions between spectral components.

The first spectral third-generation wave model developed was the Wave Model (WAM) (WAMDI Group 1988), which is still used worldwide for the simulation of waves in open ocean. This generation of models includes

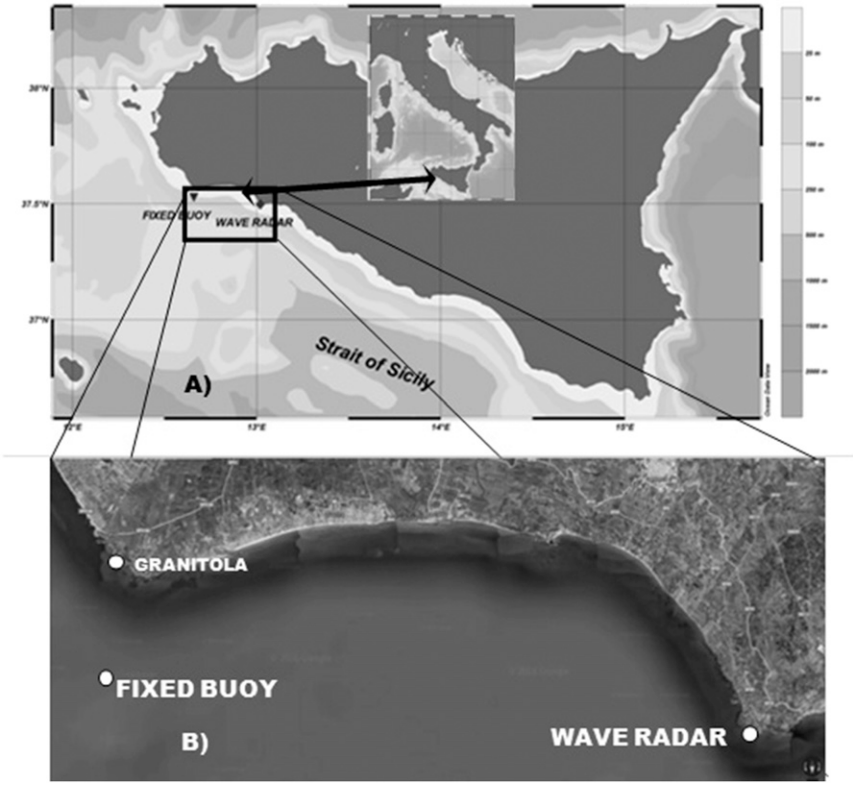

FIG. 1. (a) Map of the investigated area in the Strait of Sicily, Mediterranean Sea. (b) Relative position of the buoy and the wave radar.

the direct evaluation of nonlinear interactions without any a priori assumptions on spectral shapes. Some spectral models have been developed specifically for simulations in coastal areas and include formulations for shallow waters, among them Simulating Waves Nearshore (SWAN) (Booij et al. 1999) is one of the most used. While WAM uses an explicit numerical scheme subject to the Courant stability criterion, the SWAN formulation is based on an implicit numerical scheme that is unconditionally stable and more helpful in shallow waters. The model includes, in addition to all the formulations for deep waters present in WAM, formulations for shallow-water processes like dissipation as a result of bottom friction, triad wave–wave interactions, and depth-induced breaking. It is generally applied in nested grid simulations performed by coarser-resolution wave models.

This manuscript is devoted to the comparison of the levels of underwater noise at different frequencies with the wave heights assessed by the wave radar system and the SWAN model, in the coastal area of the Sicilian Channel (southern Italy). The innovative contribution given by the article regards the comparison between the significant wave height, measured using the X-band radar system and derived from the model, and the sound pressure level in order to discriminate natural sound sources (waves) from other sources of biological and anthropic origin, and thus have a better and quicker understanding of the effect of acoustic pollution on a marine environment. The paper is organized as follows. In section 2, the materials and methods used are introduced. Section 3 briefly presents the results achieved through the comparison of the wave height data obtained with independent information provided by the hydrophones used. Conclusions end the paper.

2. Materials and methods

a. Study area

Cape Granitola and Cape San Marco are located in the southwestern part of Sicily (see Fig. 1), in the northern part of the Sicilian Channel, in southern Italy. The channel divides the eastern from the western Mediterranean basins, which are a marine biodiversity hot spot (Myers et al. 2000). The area is affected by a series of complex oceanographic processes (Bonanno et al. 2014) that affect the high productivity of its waters

(Cuttitta et al. 2004; Patti et al. 2004), and it represents the principal corridor between the eastern and western basins with heavy and very noisy vessel traffic.

At the Cape San Marco site, a wave radar system was used as a sensor for sea surface wave measurements and a SWAN model was applied. At the Cape Granitola site, a fixed buoy was located far from the coast and was used to house a digital recording system. The two periods selected for carrying out of the research activity presented are from 28 February to 16 March 2015 and from 23 April to 27 May 2015, because that was when the hydrophone near the Cape Granitola site and the wave radar installed at the Cape San Marco site worked simultaneously.

b. Acoustic data collection and analysis

Acoustic data were collected using a digital recording system mounted on a fixed buoy having coordinates 37.51782°N, 12.65288°E located 4.9 km from the coast in front of Cape Granitola and 33 km from the radar (see Fig. 1). The buoy was fixed to the sea bottom with a semirigid antitorsion iron cable to avoid vertical oscillations caused by wave surface. A preamplifier omnidirectional hydrophone (TC 4014, Teledyne Reson, Denmark) was fixed at a depth of 20 m from the surface on a bathymetry of 48 m. The hydrophone, connected to the buoy by means of a beam, did not change position with the wave surface. The hydrophone had a flat response from 30 to 100 kHz (±2dB) with a sensitivity of −180 dB ±3 dB re 1V $(\mu\text{Pa})^{-1}$ (sensitivity of frequencies below 30 Hz is not given by the company). The hydrophone was connected to an analog–digital converter [UltraSoundGate (USG) 116H, Avisoft Bioacousics, Germany] that was managed by the software Avisoft-RECORDER (Avisoft Bioacoustics, Germany) running on an embedded PC (VIA EPIA-P720 Pico-ITX board). The data were acquired in continuous mode with a variable sampling rate of 50 000 samples per second at 16 bit. For each X-band radar sequence collected every 5 min, the power spectral density (PSD) [dB re 1 μPa^2 $(\text{Hz})^{-1}$] with the Welch's overlapped segment averaging estimator method (Welch 1967) was calculated. The calculation was made by dividing the acoustic data into Hanning windows of 2^{15} samples ($\Delta t = 0.655\,36$ s) with a signal superposition useful to the average of 2^{14} samples ($\Delta t = 0.327\,68$ s). From this PSD, the sound pressure level in the octave band (BPL, dB re 1 μPa^2) was estimated (Etter 2013).

c. Wave radar data collection and analysis

A Sperry Marine X-band radar was installed at the Cape San Marco site on a cliff at a height of about 25 m MSL. The radar antenna was located at coordinates 37.495 903°N, 13.020 878°E.

TABLE 1. Measurement parameters of the wave radar system.

Radar parameters	Value
Antenna rotation period (Δt)	2.0 s
Spatial image spacing (Δx and Δy)	4.3 m
Minimum range	200 m
Maximum range	2200 m
Image number for sequence (N_s)	64
Antenna height above sea level	~25 m
View angular sector	~190−

The radar system radiates a maximum power of 25 kW, operates in short-pulse mode (i.e., a pulse duration of about 50 ns) and is equipped with an 8-ft (2.4 m)-long antenna, with horizontal-transmit horizontal-receive (HH) polarization and a point of view of 180°. These features make it possible to get a range resolution of about 7.5 m, an angular resolution of approximately 0.9°, radar coverage of 1.20 nm and, then, a sea area monitored by the wave radar of 2.26 nm^2. The signal received by the antenna radar was converted through an analog–digital converter and interpolated onto the Cartesian grid so as to obtain 2D sea surface images. The image sequence acquired by the X-band radar was stored and processed in an elaboration unit. Each raw data sequence consists of 64 individual images, with a 2.0-s interval between successive images. The details of the Cartesian grid for the radar image are reported in Table 1.

Two main classes of inversion procedure can be used to elaborate the sequence of radar images. The first class is defined as the "global method" (Nieto Borge et al. 2004; Serafino et al. 2010) and relies on the assumption of the spatial homogeneity of sea-state parameters within the investigated area. This kind of approach can be typically applied in open sea conditions, where waves do not interact with the sea bottom and surface current circulation is not affected by the coast, so wave motion properties can be considered to be spatially homogeneous. The second class is based on the "local method" and can be applied to data acquired in nearshore areas, where the space-varying behavior of underwater topography and the presence of coastlines or coastal structures typically turns into a spatial inhomogeneity of the wave motion (Serafino et al. 2012; Ludeno et al. 2014a,b; Bell 2008; Senet et al. 2008).

Hereinafter, the local method proposed in Ludeno et al. (2014b, 2015) and Brandini et al. (2017) was adopted to deal with the reconstruction of inhomogeneous surface current fields from X-band radar data. Figure 2

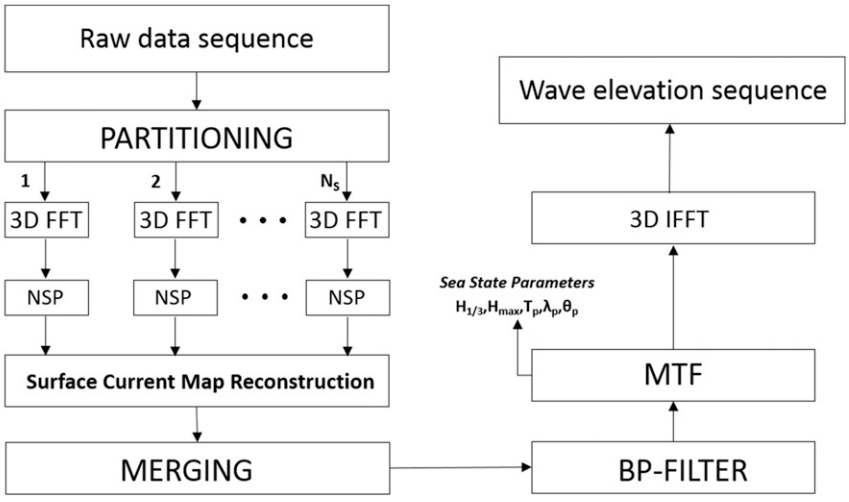

FIG. 2. Block diagram of the inversion procedure.

illustrates the block diagram of the inversion procedure and can be summarized as follows. Each radar image belonging to the temporal sequence considered is partitioned into N_s spatially overlapping subareas, giving rise to N_s temporal subsequences. After data partitioning, N_s radar spectra, each relevant to a given subarea, are computed via the FFT algorithm (Ludeno et al. 2014a,b, 2015).

Each spectrum $\{F^j(\mathbf{k},\omega)\}_{j=1,\ldots,N_s}$, where $\mathbf{k}=(k_x, k_y)$ is the wave vector and ω is the angular frequency, is then processed via the NSP method (Serafino et al. 2010) so as to retrieve the local surface current vector through the following estimator:

$$V^j(\mathbf{U}) = \arg\max_h \frac{\langle |F^j(\mathbf{k},\omega)|, G(\mathbf{k},\omega,\mathbf{U})\rangle}{\sqrt{P_F P_G}}, \qquad (1)$$

where $G(\mathbf{k}, \omega, \mathbf{U}) = \delta(\omega - \sqrt{gk} - \mathbf{k}\cdot\mathbf{U})$ is the characteristic function [where $\delta(\cdot)$ is the Dirac delta distribution] based on the dispersion relation, $\langle |F|, G\rangle$ represents the scalar product between the functions $|F|$ and G, and P_F and P_G are the powers associated with $|F|$ and G, respectively. In particular, using the local version of NSP, the surface current field can be easily computed and its value is used to define the global (applied to the whole radar spectrum) BP filter (Serafino et al. 2012; Ludeno et al. 2014a,b). To this aim, the merging block provides the intervals containing the effective values for the currents and bathymetry of the whole area examined. Based on these intervals, it is possible to identify the (ω, k) domain containing the energy of the overall sea signal and the spectral representation of the band-pass filter. The desired sea wave spectrum $F_w(\mathbf{k}, \omega)$ can be obtained from the filtered image spectrum $\tilde{F}_I(\mathbf{k}, \omega)$ by resorting to the radar MTF used to mitigate the distortions introduced in the radar imaging process (Nieto Borge et al. 2004; Fucile et al. 2016). Herein, we adopt the MTF already used to monitor the sea state in the coastal area in front of Giglio Island (Ludeno et al. 2014a) and reported in Eq. (2):

$$\mathrm{MTF} \propto \begin{cases} k^2 & \text{for} \quad k > \pi/30 \\ k^{-1.8} & \text{for} \quad \pi/30 \le k \end{cases}, \qquad (2)$$

where $k = |\mathbf{k}| = \sqrt{k_x^2 + k_y^2}$.

The knowledge of the 3D wave spectrum $F_w(\mathbf{k}, \omega)$ makes it possible to determine the main sea-state parameters; this is performed by generating the wavenumber directional spectrum $F(\mathbf{k})$, from which the wavelength (λ_p), the direction (θ_p), and the period (T_p) of the dominant waves can then be retrieved. In particular, the significant wave height H_s is computed from the 3D sea wave spectrum $F_w(k_x, k_y, \omega)$ with the following equation (Nieto Borge et al. 2008):

$$H_s = 4\sqrt{\int_{\mathbf{k},\omega} F_w(k_x, k_y, \omega)\, dk_x\, dk_y\, d\omega}. \qquad (3)$$

Finally, the sea wave sequence can be easily reconstructed from the 3D wave spectrum by exploiting the inverse fast Fourier transform (IFFT) algorithm.

d. SWAN model

An operational wave forecast system for the entire Mediterranean basin has been running at ENEA since June 2013. The system provides daily 5-day forecasts, starting at time 0000 UTC. The simulations are performed with a parallel version of WAM cycle 4.5.3

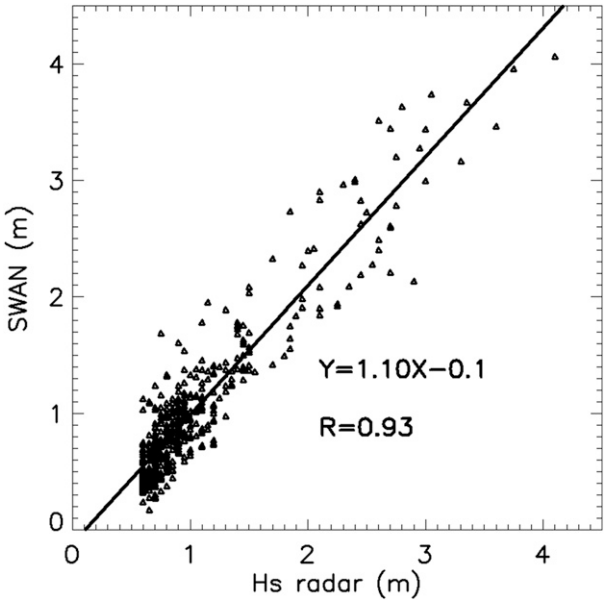

FIG. 3. Linear correlation between H_s radar and SWAN model wave height. The black line in the scatterplot represents the regression line, whose equation is provided in the lower-right part of the panel.

(Günther and Behrens 2011) at the resolution of 1/32° in each direction, corresponding to a linear mesh size of about 3.5 km. Hourly wave spectra are used to force laterally higher-resolution simulations for an area in the northwestern edge of Sicily stretching from longitude 12.625° to 13.375°E and from latitude 37.16875° to 37.66875°N. For these simulations a SWAN model (Booij et al. 1999) at a horizontal resolution of 1/124° was applied. Model bathymetry was calculated from the General Bathymetric Chart of the Oceans (GEBCO) 30-arc-s gridded dataset (http://www.gebco.net/data_and_products/gridded_bathymetry_data). The initial conditions for each wave simulation were obtained as a restart from the simulation of the previous day.

The directional wave energy density spectrum for both the WAM and SWAN models was discretized using 36 directional bins, corresponding to an angular resolution of 10°, and 32 frequency bins starting from 0.06 Hz with relative size increments of 0.1 between one frequency bin and the next.

The entire forecast system composed of the WAM and SWAN models is forced with hourly wind fields obtained from the meteorological operational system SKIRON, developed by the Atmospheric Modeling and Weather Forecasting Group of the University of Athens (Kallos et al. 1997). The atmospheric model is run daily over the Mediterranean basin at the horizontal resolution of 0.05° × 0.05°.

The main wave-integrated variables, including significant wave height, mean, and peak wave period and wave direction, for each grid point of the computational domain of both the models were stored hourly. A validation of the significant wave heights produced by the operational system was achieved against data derived from satellite measurements over the period June 2013–November 2014 (Carillo et al. 2015).

In the study presented, the significant wave heights at buoy position are extracted from the first day of the forecast performed using the SWAN model. To evaluate the comparison with the hydrophone's measurements, the time series values for the H_s higher than 0.5 m estimated by the SWAN model and

TABLE 2. Median values (10th and 90th percentiles) and R values for the linear correlation analysis between significant wave height from radar and the model, and BPLs at different frequency bands (the p values of the correlation are always <0.001). The measure of the goodness of fit of the linear regression is denoted by R, and p values are the significance of the test for linear regression.

				Radar wave height (m)	SWAN model wave height (m)
	Median	10th percentile	90th percentile	R	R
Radar wave height (m)	0.80	0.60	1.85	1.00	0.93
SWAN model wave height (m)	0.77	0.40	1.90	0.93	1.00
16 Hz	108.95	101.07	123.03	0.79	0.82
31.5 Hz	106.80	99.92	119.26	0.77	0.82
63 Hz	111.16	102.17	121.99	0.69	0.73
125 Hz	107.48	100.24	120.33	0.75	0.77
250 Hz	99.86	93.73	108.90	0.68	0.64
500 Hz	96.39	92.09	105.72	0.50	0.44
1000 Hz	94.91	89.15	102.30	0.43	0.37
2000 Hz	92.80	87.63	100.72	0.55	0.50
4000 Hz	90.56	86.66	96.38	0.54	0.49
8000 Hz	89.93	87.68	94.05	0.60	0.58
16 000 Hz	91.00	89.87	92.53	0.58	0.59

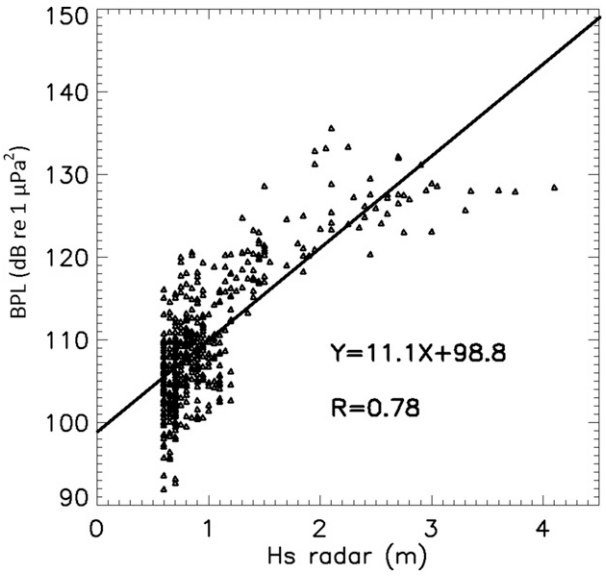

FIG. 4. Linear correlation between 16-Hz BPL and H_s radar. The black line in the scatterplot represents the regression line, whose equation is provided in the lower-right part of the panel.

measured from the wave radar were adequately selected. Because of the relative distance (about 19 nm) between the position of the buoy and the middle of the sea area of 2.26 nm^2 monitored by the wave radar, the trend of the H_s values by the SWAN model in both positions was calculated. The two series of data are found to be well linearly correlated with a goodness-of-fit R^2 value equal to 0.97 (not shown); thus, for convenience, the model values calculated at the position related to the radar was used for statistical analysis and graphs.

e. *Statistical analysis*

The statistical analysis was performed on three time series data: radar significant wave height, model significant wave height, and acoustic noise at different octave bands. Since in a lower sea-state condition [i.e., significant wave height smaller than 0.5 m (<level 3 on the Douglas scale)] radar images do not allow a reliable estimation (Ludeno et al. 2016; Raffa et al. 2017), in this study only radar data estimating wave heights higher than 0.5 m were considered. In particular, the H_s values ranged from 0.5 to 4 m. Since the data were not normally distributed, the median and 10% and 90% percentiles were calculated. A linear correlation was carried out to compare the radar significant wave height, the model significant wave height (used to validate the radar measurements), and acoustic noise at different octave bands. Hereinafter, R is the measure of the goodness of fit of the linear correlation and p values are the significance of the test for linear correlation. The analysis was performed in Statistica, version 8 (United States). Furthermore, in order to have a more detailed view, the correlation between each frequency from 1 to 16 Hz (PSD, dB re 1 $\mu Pa^2\,Hz^{-1}$) and the significant wave height was assessed. A mean PSD for each different sea state, as assessed by the significant wave heights intensity (H_s radar), was calculated.

3. Results

The radar measurements and the SWAN model estimates obtained are well correlated with an R value greater than 0.9 (Fig. 3). Table 2 reports the median values (with 10% and 90% percentiles) of H_s from the

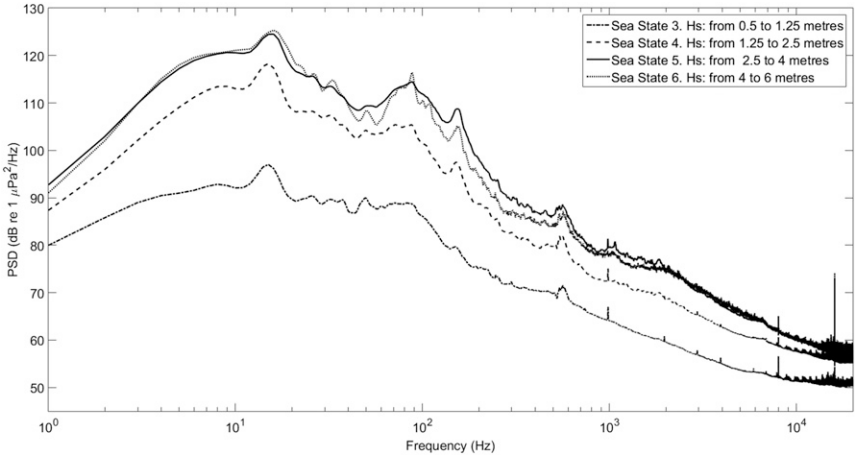

FIG. 5. Mean of power spectral density (dB re 1 $\mu Pa^2\,Hz^{-1}$) for different sea states obtained by H_s radar. The PSD for the frequencies below 30 Hz is not calibrated. Total number of files = 681. Number of files used to calculate the curve of the following: sea state 3 = 571; sea state 4 = 89; sea state 5 = 20; sea state 6 = 1.

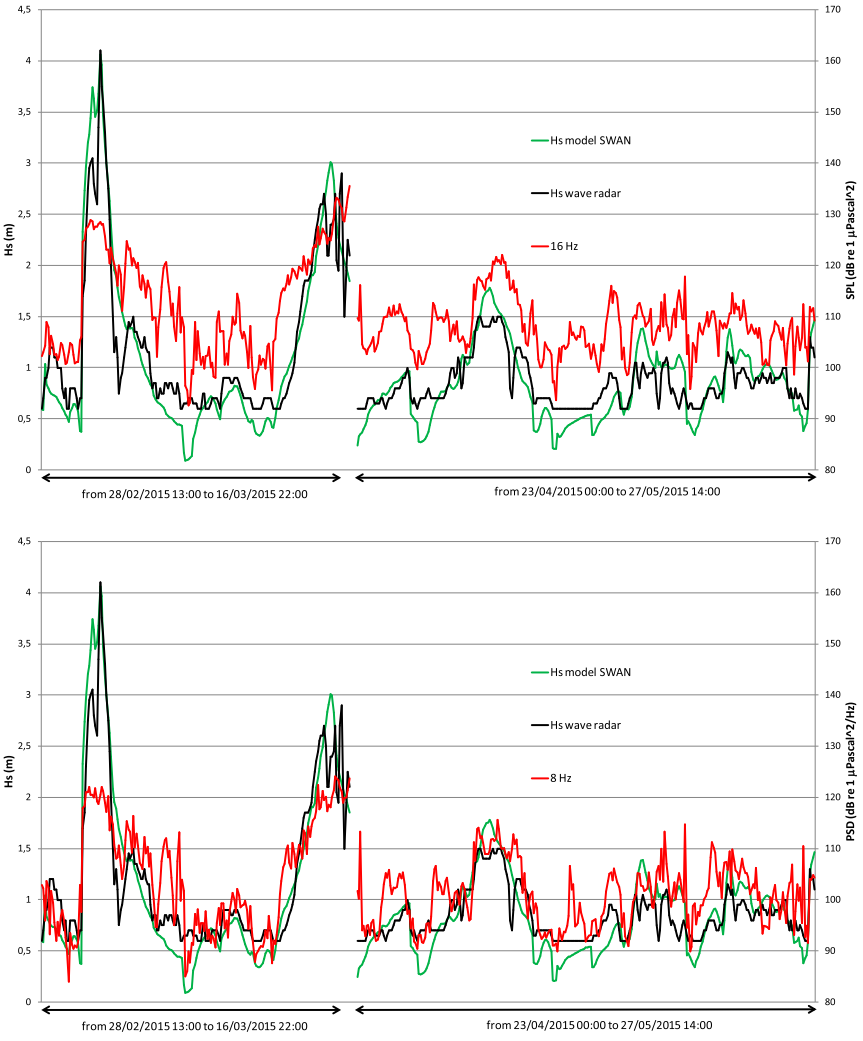

FIG. 6. (top) The significant wave height H_s from wave radar and from the SWAN model at radar position, and BPL at 16 Hz. (bottom) Same H_s values as for (top), but PSD at 8 Hz.

radar and SWAN model assessments (0.80 ± percentile and 0.70 ± percentile, respectively) and the acoustic BPL for the whole period. In this table, the R and p values of the correlation between the measurements of the three different technologies are shown. The R values increase for lower BPLs and exhibit the best correlation with a wave height ($R = 0.78$ for the radar measurements) at 16 Hz (Fig. 4).

The highest value of correlation between PSD from 1 to 16 Hz and radar wave height was revealed at 8 Hz ($R = 0.8$). At the lowest frequencies up to 200 Hz, the sea state was characterized by a higher level of noise compared to that at the higher frequencies (Fig. 5). Furthermore, the increase in sea state produced a considerable increase in noise at the lower frequencies (below 200 Hz) in comparison with that at the higher frequencies (Fig. 5). Figure 6 shows the time series of the H_s estimated by the radar data coupled with the acoustic data at 16 Hz (BPL) and 8 Hz (PSD) (Fig. 6, top and bottom, respectively) and the SWAN model.

4. Discussion and conclusions

This research work is focused on investigating the correlation of underwater noise on the significant wave heights assessed by radar methodology in an area of the Sicilian Channel. In situ acoustic data from a fixed observing system were coupled with significant wave height estimates provided by the coastal wave radar system installed at Cape San Marco and with reliable estimates from a SWAN model.

The results of the analysis of the acoustic data collected by a digital recording system installed at a depth of about 20 m were presented. The estimates provided by the SWAN model were compared to the wave radar measurements available over the coastal location. The comparison showed good linear correlation with a correlation coefficient greater than 0.9. The acoustic underwater noise analysis exhibited good correspondence with wave radar measurements and the SWAN model with a high R value of 0.78 and 0.82, respectively; however, at higher wave heights, the PSD seems to be underestimated (Fig. 6 for 8 Hz PSD). This is due to the intrinsic nature of the logarithmic scale (dB). The PSD peak values (Fig. 6 for 8-Hz PSD) cannot be explained by the wave height; these peaks are dependent on other sound sources in the sea (biological sound, anthropogenic pollution). Given the duration and the power, it seems more likely that these peaks were caused by vessel traffic. Biological sound sources, in fact, are usually less powerful and have a shorter duration. The PSD curves in Fig. 5 show that noise increase at lower frequencies depends on the wave height measured by radar. Radar technologies could be employed to assess the mean natural sound levels in a specific shallow-water sea area for each different sea state. Possible discrepancies of the PSD with the mean acoustics sea-state level could be attributed to other sources, such as vessel traffic or biological activities.

In the light of the results discussed above, it could be very useful to assimilate an integrated system with radar/acoustic measurements into the early warning systems in the Mediterranean Sea coastal areas of Italy for the monitoring of noise levels. Furthermore, to discriminate the anthropogenic sound sources from other sources in coastal areas, an automatic identification system (AIS) and/or radar for vessel tracking should be used. This experiment is still ongoing and the latest data acquired will be used for further analysis on the parameterization of both wave and noise, and new tests will be carried out to improve the capability of wave radar to distinguish a more complete set of different sources of oceanic noise.

Acknowledgments. The authors express sincere appreciation to the CNR IAMC UOS team in Cape Granitola (P. Calandrino, I. Fontana, and G. Giacalone) for having supported the installation of the radar systems and the experimental activities. Most of the research work leading to this paper was carried out within the framework of the RITMARE Flagship Project, funded by the Italian Ministry of University and Research.

REFERENCES

Bell, P. S., 2008: Mapping shallow water coastal areas using a standard marine X-band radar. *16th European Hydro Conf. (Hydro8)*, Liverpool, United Kingdom, Hydrographic Society UK, Paper 4 http://nora.nerc.ac.uk/id/eprint/5938.

Bonanno, A., and Coauthors, 2014: Variability of water mass properties in the Strait of Sicily in summer period of 1998–2013. *Ocean Sci.*, **10**, 759–770, https://doi.org/10.5194/os-10-759-2014.

Booij, N., R. C. Ris, and L. H. Holthuijsen, 1999: A third-generation wave model for coastal regions: 1. Model description and validation. *J. Geophys. Res.*, **104**, 7649–7666, https://doi.org/10.1029/98JC02622.

Brandini, C., S. Taddei, B. Doronzo, M. Fattorini, L. Costanza, M. Perna, F. Serafino, and G. Ludeno, 2017: Turbulent behaviour within a coastal boundary layer, observations and modelling at the Isola del Giglio. *Ocean Dyn.*, **67**, 1163–1178, https://doi.org/10.1007/s10236-017-1080-1.

Buscaino, G., and Coauthors, 2010: Impact of an acoustic stimulus on the motility and blood parameters of European sea bass (*Dicentrarchus labrax* L.) and gilthead sea bream (*Sparus aurata* L.). *Mar. Environ. Res.*, **69**, 136–142, https://doi.org/10.1016/j.marenvres.2009.09.004.

——, and Coauthors, 2016: Temporal patterns in the soundscape of the shallow waters of a Mediterranean marine protected area. *Sci. Rep.*, **6**, 34230, https://doi.org/10.1038/srep34230.

Carillo, A., G. Sannino, and E. Lombardi, 2015: Wave energy potential: A forecasting system for the Mediterranean basin. Ocean energy: Ongoing research in Italy, ENEA EAI Speciale II-2015, 16–21, https://doi.org/10.12910/EAI2015-053.

Carratelli, E. P., F. Dentale, and F. Reale, 2007: Reconstruction of SAR wave image effects through pseudo random simulation. *Proc. Envisat Symp. 2007*, Montreaux, Switzerland, European Space Agency SP-636, 508120, http://envisat.esa.int/envisatsymposium/proceedings/posters/2P1/508120pu.pdf.

Celi, M., and Coauthors, 2016: Vessel noise pollution as a human threat to fish: Assessment of the stress response in gilthead seabream (*Sparus aurata*, Linnaeus 1758). *Fish Physiol. Biochem.*, **42**, 631–641, https://doi.org/10.1007/s10695-015-0165-3.

Cotter, A. J. R., 2009: The ''soundscape'' of the sea, underwater navigation, and why we should be listening more. *Advances in Fisheries Science: 50 Years on from Beverton and Holt*, A. I. L. Payne, J. Cotter, and T. Potter, Eds., Wiley, 451–471.

Cuttitta, A., and Coauthors, 2004: Mesopelagic fish larvae species in the Strait of Sicily and their relationships to main oceanographic events. *Hydrobiologia*, **527**, 177–182, https://doi.org/10.1023/B:HYDR.0000043299.65829.2f.

Etter, P. C., 2013: *Underwater Acoustic Modeling and Simulation*. 4th ed. CRC Press, 544 pp.

European Parliament, Council of the European Union, 2008: Directive 2008/56/EC establishing a framework for community action in the field of marine environmental policy (Marine Strategy Framework Directive). *Off. J. Eur. Union,* **51**, 19–40, OJL-164, http://data.europa.eu/eli/dir/2008/56/oj.

Filiciotto, F., and Coauthors, 2014: Behavioural and biochemical stress responses of *Palinurus elephas* after exposure to boat noise pollution in tank. *Mar. Pollut. Bull.*, **84**, 104–114, https://doi.org/10.1016/j.marpolbul.2014.05.029.

Fucile, F., G. Ludeno, F. Serafino, G. Bulian, F. Soldovieri, and C. Lugni, 2016: Some challenges in recovering wave features from a wave radar system. *Proc. 26th Int. Ocean and Polar Engineering Conf. (ISOPE)*, International Society of Offshore

and Polar Engineers, Rhodes, Greece, 319, http://www.isope.org/publications/proceedings/ISOPE/ISOPE%202016/papers/16TPC-0698.pdf.

Gangeskar, R., 2014: An algorithm for estimation of wave height from shadowing in X-band radar sea surface images. *IEEE Trans. Geosci. Remote Sens.*, **52**, 3373–3381, https://doi.org/10.1109/TGRS.2013.2272701.

Günther, H., and A. Behrens, 2011: The WAM model validation document version 4.5.3. Helmholtz-Zentrum Geesthacht Tech. Rep., 20 pp.

Haxel, J. H., R. P. Dziak, and H. Matsumoto, 2013: Observations of shallow water marine ambient sound: The low frequency underwater soundscape of the central Oregon coast. *J. Acoust. Soc. Amer.*, **133**, 2586–2596, https://doi.org/10.1121/1.4796132.

Hildebrand, J. A., 2009: Anthropogenic and natural sources of ambient noise in the ocean. *Mar. Ecol. Prog. Ser.*, **395**, 5–20, https://doi.org/10.3354/meps08353.

Huang, W., and E. Gill, 2012: Surface current measurement under low sea state using dual polarized X-band nautical radar. *IEEE J. Sel. Top. Appl. Earth Obs. Remote Sens.*, **5**, 1868–1873, https://doi.org/10.1109/JSTARS.2012.2208179.

Kallos, G. B., and Coauthors, 1997: The regional weather forecasting system SKIRON. *Proceedings of the Symposium on Regional Weather Prediction on Parallel Computer Environments*, G. B. Kallos et al., Eds., University of Athens, 109–122.

Lee, P. H. Y., and Coauthors, 1995: X band microwave backscattering from ocean waves. *J. Geophys. Res.*, **100**, 2591–2611, https://doi.org/10.1029/94JC02741.

Liu, X., W. Huang, and E. W. Gill, 2016: Comparison of wave height measurement algorithms for ship-borne X-band nautical radar. *Can. J. Remote Sens.*, **42**, 343–353, https://doi.org/10.1080/07038992.2016.1177450.

Ludeno, G., C. Brandini, C. Lugni, D. Arturi, A. Natale, F. Soldovieri, B. Gozzini, and F. Serafino, 2014a: Remocean system for the detection of the reflected waves from the Costa Concordia ship wreck. *IEEE J. Sel. Top. Appl. Earth Obs. Remote Sens.*, **7**, 3011–3018, https://doi.org/10.1109/jstars.2014.2321048.

——, S. Flampouris, C. Lugni, F. Soldovieri, and F. Serafino, 2014b: A novel approach based on marine radar data analysis for high-resolution bathymetry map generation. *IEEE Geosci. Remote Sens. Lett.*, **11**, 234–238, https://doi.org/10.1109/LGRS.2013.2254107.

——, F. Reale, F. Dentale, E. P. Carratelli, A. Natale, F. Soldovieri, and F. Serafino, 2015: An X-band radar system for bathymetry and wave field analysis in a harbour area. *Sensors*, **15**, 1691–1707, https://doi.org/10.3390/s150101691.

——, C. Nasello, F. Raffa, G. Ciraolo, F. Soldovieri, and F. Serafino, 2016: A comparison between drifter and X-band wave radar for sea surface current estimation. *Remote Sens.*, **8**, 695, https://doi.org/10.3390/rs8090695.

Lund, B., C. O. Collins, H. C. Graber, E. Terrill, and T. H. C. Herbers, 2014: Marine radar ocean wave retrieval's dependency on range and azimuth. *Ocean Dyn.*, **64**, 999–1018, https://doi.org/10.1007/s10236-014-0725-6.

Maccarrone, V., F. Filiciotto, G. de Vincenzi, S. Mazzola, and G. Buscaino, 2015: An Italian proposal on the monitoring of underwater noise: Relationship between the EU Marine Strategy Framework Directive (MSFD) and marine spatial planning directive (MSP). *Ocean Coastal Manage.*, **118B**, 215–224, https://doi.org/10.1016/j.ocecoaman.2015.07.006.

Myers, N., R. A. Mittermeier, C. G. Mittermeier, G. A. B. da Fonseca, and J. Kent, 2000: Biodiversity hotspots for conservation priorities. *Nature*, **403**, 853–858, https://doi.org/10.1038/35002501.

Nieto Borge, J. C., 1997: Análisis de campos de oleaje mediante radar de navegación en Banda X. Ph.D. thesis, Universidad de Alcalá de Henares, 320 pp.

——, and C. Guedes Soares, 2000: Analysis of directional wave fields using X-band navigation radar. *Coastal Eng.*, **40**, 375–391, https://doi.org/10.1016/S0378-3839(00)00019-3.

——, G. Rodríquez Rodríguez, K. Hessner, and P. I. González, 2004: Inversion of marine radar images for surface wave analysis. *J. Atmos. Oceanic Technol.*, **21**, 1291–1300, https://doi.org/10.1175/1520-0426(2004)021<1291:IOMRIF>2.0.CO;2.

——, K. Hessner, P. Jarabo-Amores, and D. De La Mata-Moya, 2008: Signal-to-noise ratio analysis to estimate ocean wave heights from X-band marine radar image time series. *IET Radar, Sonar Navig.*, **2**, 35–41, https://doi.org/10.1049/iet-rsn:20070027.

Nystuen, J. A., 1986: Rainfall measurements using underwater ambient noise. *J. Acoust. Soc. Amer.*, **79**, 972–982, https://doi.org/10.1121/1.393695.

Patti, B., and Coauthors, 2004: Interannual fluctuations in acoustic biomass estimates and in landings of small pelagic fish populations in relation to hydrology in the Strait of Sicily. *Chem. Ecol.*, **20**, 365–375, https://doi.org/10.1080/02757540410001727972.

Plant, W. J., and W. C. Keller, 1990: Evidence of Bragg scattering in microwave Doppler spectra of sea return. *J. Geophys. Res.*, **95**, 16 299–16 310, https://doi.org/10.1029/jc095ic09p16299.

Prosperetti, A., and H. N. Oguz, 1993: The impact of drops on liquid surfaces and the underwater noise of rain. *Annu. Rev. Fluid Mech.*, **25**, 577–602, https://doi.org/10.1146/annurev.fl.25.010193.003045.

Pugliese Carratelli, E., F. Dentale, and F. Reale, 2006: Numerical pseudo-random simulation of SAR sea and wind response. *Proc. SEASAR 2006: Advances in SAR Oceanography from Envisat and ERS Missions*, Frascati, Italy, European Space Agency SP-613, http://earth.esa.int/workshops/seasar2006/proceedings/papers/p7_pugli.pdf.

Raffa, F., G. Ludeno, B. Patti, F. Soldovieri, S. Mazzola, and F. Serafino, 2017: X-band wave radar for coastal upwelling detection off the southern coast of Sicily. *J. Atmos. Oceanic Technol.*, **34**, 21–31, https://doi.org/10.1175/JTECH-D-16-0049.1.

Salcedo-Sanz, S., J. C. Nieto Borge, L. Carro-Calvo, L. Cuadra, K. Hessner, and E. Alexandre, 2015: Significant wave height estimation using SVR algorithms and shadowing information from simulated and real measured X-band radar images of the sea surface. *Ocean Eng.*, **101**, 244–253, https://doi.org/10.1016/j.oceaneng.2015.04.041.

Sarà, G., and Coauthors, 2007: Effect of boat noise on the behaviour of bluefin tuna *Thunnus thynnus* in the Mediterranean Sea. *Mar. Ecol. Prog. Ser.*, **331**, 243–253, https://doi.org/10.3354/meps331243.

Senet, C. M., J. Seemann, and F. Ziemer, 2001: The near-surface current velocity determined from image sequences of the sea surface. *IEEE Trans. Geosci. Remote Sens.*, **39**, 492–505, https://doi.org/10.1109/36.911108.

——, ——, S. Flampouris, and F. Ziemer, 2008: Determination of bathymetric and current maps by the method DiSC based on the analysis of nautical X-band radar image sequences of the sea surface (November 2007). *IEEE Trans. Geosci. Remote Sens.*, **46**, 2267–2279, https://doi.org/10.1109/TGRS.2008.916474.

Serafino, F., C. Lugni, and F. Soldovieri, 2010: A novel strategy for the surface current determination from marine X-band radar data. *IEEE Geosci. Remote Sens. Lett.*, **7**, 231–235, https://doi.org/10.1109/LGRS.2009.2031878.

——, and Coauthors, 2012: REMOCEAN: A flexible X-band radar system for sea-state monitoring and surface current estimation. *IEEE Geosci. Remote Sens. Lett.*, **9**, 822–826, https://doi.org/10.1109/LGRS.2011.2182031.

Shen, C., W. Huang, E. W. Gill, R. Carrasco, and J. Horstmann, 2015: An algorithm for surface current retrieval from X-band marine radar images. *Remote Sens.*, **7**, 7753–7767, https://doi.org/10.3390/rs70607753.

Vicen-Bueno, R., C. Lido-Muela, and J. C. Nieto Borge, 2012: Estimate of significant wave height from non-coherent marine radar images by multilayer perceptrons. *EURASIP J. Adv. Signal Process.*, **2012**, 84, https://doi.org/10.1186/1687-6180-2012-84.

WAMDI Group, 1988: The WAM Model—A third generation ocean wave prediction model. *J. Phys. Oceanogr.*, **18**, 1775–1810, https://doi.org/10.1175/1520-0485(1988)018<1775:TWMTGO>2.0.CO;2.

Welch, P., 1967: The use of fast Fourier transform for the estimation of power spectra. *Audio Electroacoust. IEEE Trans.*, **15**, 70–73, https://doi.org/10.1109/TAU.1967.1161901.

Wenzel, L. B., 1990: Electromagnetic scattering from the sea at low grazing angles. *Surface Waves and Fluxes: Remote Sensing*, G. L. Geernaert and W. L. Plant, Eds., Environmental Fluid Mechanics, Vol. 8, Kluwer Academic, 109–172, https://doi.org/10.1007/978-94-009-0627-3_3.

Young, I. R., W. Rosenthal, and F. Ziemer, 1985: A three-dimensional analysis of marine radar images for the determination of ocean wave directionality and surface currents. *J. Geophys. Res.*, **90**, 1049–1059, https://doi.org/10.1029/JC090iC01p01049.